Seismoprogn. Observ. Territ. Azerb. V.12, №1, 2015, pp.3-18

MOMENT MAGNITUDES OF LOCAL/REGIONAL EVENTS FROM 1-D CODA CALIBRATIONS IN THE BROADER MIDDLE EAST REGION

R.Gok[1], A.Kaviani[2], E.M.Matzel[1], M.E.Pasyanos[1], K.Mayeda[3], G.Yetirmishli[4], I.El-Hussain[5], A.Al-Amri[6], A.Al-Enezi[7], T.Godoladze[8], D.Kalafat[9], E.A.Sandvol[10], W.R.Walter[1]

ABSTRACT. Short-period body wave and long-period surface wave magnitudes are important for event characterization, and yield estimation applications. However, the uneven distribution of stations, complex heterogeneous structure, and high attenuation of the Middle East make it difficult to calculate these magnitudes using simple 1-D path corrections. While reliable 1-D long-period regional moment magnitudes are routinely computed for the larger magnitude events, oftentimes the smaller events do not have the required bandwidth and are thus not suitable for long-period waveform modeling that require periods of 5 seconds or greater. The complex structure of the lithosphere in the region causes significant variation in the recorded amplitude of body and surface waves that travel along different paths, as well as phase blockage. These strong 2-D effects are most significant for source characterization of small and moderate magnitude events, which are often only observable at periods of less than 2 seconds. While the regional coda envelope method for moment magnitude estimation [22] has proven to be very robust in many studies, they still require 2-D path corrections for the shorter periods in laterally complex regions Iranian and Turkish Plateaus. This current study will provide the necessary 1-D initial starting model for use in a future 2-D coda study. We are also very fortunate to have access to many new broadband stations that have become available in the region, through improved national networks as well as temporary deployments. This has given us the opportunity to make thousands of coda amplitude measurements to calculate source parameters, specifically we have estimated the source moment-rate spectra and moment magnitudes for roughly 2,900 events recorded by 74 stations over 13 narrow frequency bands ranging between 0.03-8 Hz. Moreover, this data will be crucial for 2-D path corrections for coda in the future. The absolute scaling of these spectra was calculated based on an independent waveform modeling solutions of the moment magnitudes for a subset of these events to avoid circularity. Using our1-D path calibrations, we obtain fairly good agreement with waveform-modeled seismic moments for the larger events (Mw > 4.5), for the low frequencies (< 0.7 Hz). As expected, the coda-derived source spectra become very scattered at higher frequencies (>0.7-Hz) because of uncorrected 2-D path effects as well as mixing of both Sn-coda and Lg-coda which are likely to have different attenuation.

Introduction

Moment magnitude estimation in tectonically diverse regions is very challenging due to the effects of strong structural variations that cannot be simply modeled with 1-D velocity structure. In this study we utilize national network data to enable better estimates of seismic source parameters in the broader Middle East region. For sparse local and regional seismic networks, a stable moment magnitude is quite important for establishing accurate seismicity catalogs and assessing seismic hazard

[1]*Lawrence Livermore National Laboratory,*
[2]*University of Frankfurt,*
[3]*Weston Geophysical,*
[4]*Azerbaijan National Academy of Sciences,*
[5]*Sultan Qaboos University,*
[6]*King Saud University,*
[7]*Kuwait Institute for Scientific Research,*
[8]*Ilia State University,*
[9]*Kandilli Observatory and Earthquake Research Institute,*
[10]*University of Missouri,*

potential. Accurate magnitude and source parameters are also critical for construction and formation of regional attenuation parameters. Unlike other types of magnitudes such as M_L, M_b and M_s which often have biases due to regional propagation differences, the empirical coda envelope approach [21; 22] can provide stable, absolute source spectra that are corrected for S-to-coda transfer function, scattering, inelastic attenuation and site effects. In previous studies, we found that the coda envelope amplitude measurements were not very sensitive to 3-D path heterogeneity (at lower frequencies) and source radiation pattern provided ample duration was available for the coda amplitude measurements [24]. Due to the scattering nature of the coda, amplitudes derived from the envelopes average over the path and source variation. The resultant source spectra were used to calculate stable moment estimates (and hence Mw), and the comparison between traditional magnitudes (M_L, M_b and M_s) as well radiated seismic energy. In this study we use the 1-D coda-derived spectra that is dominated by scattered surface waves at longer periods and scattered Sn and/or Lg waves at regional distances, as well as scattered direct S wave sat local distances. Our goal is to provide a large set of calibrated quality assessed moment magnitudes of nearly 2,900 small to large size earthquakes that would span 3.5<Mw<7.0.

Although the coda envelopes are robust for larger range of frequencies for regional phases (above 0.7 Hz) their characteristics would still influence the coda envelope calibrations. The *Sn* phase is a high-frequency guided seismic wave that travels in the lithospheric mantle with a typical frequency of 1 to 4 Hz or more. The typical velocity for *Sn* is around 4.5 km s^{-1} in stable continental and oceanic lithosphere. *Lg* is shown to be sensitive to lateral changes in the crust and travels with 3.7-3.2 km s^{-1}. These variations will effect the 1-D coda start time calibrations as will be demonstrated well in the method section.

The Lg coda typically constitutes the most prominent phase observed on regional-distance seismograms recorded from crustal events traveling over continental paths. Lg coda is widely used for local and regional attenuation studies for stable Q estimates [3; 8]. In active tectonic regions direct Lg waves are highly attenuated. Molnar and Oliver (1969) followed by Kadinsky-Cade et al (1981) observed very weak Sn propagation in the Iranian-Turkish Plateau. The same study demonstrates that Lg is also absent or weak on the seismograms with paths crossing the Plateau and across the South Caspian Sea. Later studies by Mitchell et al (1997), Rodgers et al (1997) and Cong and Mitchell (1998) confirmed the same results (Figure 1a). The more detailed studies by Sandvol et al (2001), Gök et al (2003) and Al-Damegh et al (2006) indicate Lg blockage across the Bitlis Suture and the Zagros fold and thrust belt and weak Lg and Sn propagation in most part of the Iranian-Turkish Plateau (Baumgardt, 2001)(Figure 1). Kaviani et al (2015) present detailed crustal attenuation and velocity models for the Northern Middle East by analysis of Lg waves recorded at very dense network.The tomographic models presented by Kaviani et al. (2015) show lower values of Lg Q_0 over the Turkish-Anatolian Plateau (<150) than those observed over the Iranian Plateau (150-400).

Direct wave amplitude measurements are affected by source radiation pattern, directivity and heterogeneities along the path which causes large amplitude variability (e.g. Favreau and Archuleta 2003). Previous studies have compared direct waves with coda waves [20; 21; 22; 10; 19] and all have found that amplitude measurements of direct waves are 3 to 5 times more variable than coda amplitudes. We demonstrate in this study that 1-D coda-derived magnitudes provide great stability due to their averaging nature for longer periods and thus are applicable for events Mw >= ~4.0 for this region.

However, for smaller events it is clear that 2-D path effects become significant and a simple 1-D path correction is not adequate. This study will provide an initial starting model for a future 2-D coda amplitude tomography that we believe will allow for stable moment magnitudes down to Mw=3.0 or lower. The 1-D coda calibration technique is also powerful with rather easy and robust for national networks for operational purposes when a local monitoring organization is required to report Mw.

Data

We analyzed waveforms from 74 seismic stations consisting of permanent and temporary stations in the region (Fig. 1b). All stations were three-component broadband from national networks or open data sources (wherever available). Station-selection criteria was also based on geographical distribution and homogeneity. Since coda waves provide an averaging effect along the path, many studies showed that even single station moment magnitudes are very close to the network average of direct waves [21]. We obtained a large number of crustal (h<33km) events out to ~14 degrees where most of the seismic activity is associated with major plate boundaries or the Turkish and Iranian Plateaus (e.g., Bitlis-Zagros Fold and Trust Belt, Red Sea, Makran). The majority of the data comes from seismic monitoring centers such as national networks or openly available permanent and temporary deployments. We used the preferred origin information for each event from our database. In the Arabian Peninsula, there are limited number of events and subsequently did not provide much data due to distance limitations and attenuation. IRIS-PASSCAL deployments, IIEES (Iranian Institute of Earthquake Engineering), Republican Seismic Survey Center of Azerbaijan (RSSC), Earthquake Monitoring Center (EMC) of Sultan Qaboos University, KACST (King Abdullah City of Science and Technology), Kandilli Observatory and Earthquake Research Institute (KOERI), Kuwait Institute for Scientific Research (KISR) and Saudi Geological Survey (SGS) provided the most complete coverage for any study that involve so many institutions and data in the broader Middle East region.

Method

Instrument corrected regional broadband velocity seismograms were used in the coda calibration following the method outlined by Mayeda et al., [21, 22]. The result is coda-derived moment-rate spectra that are tied to independent waveform modeled moments. The coda technique described here has been widely used for regional calibrations that even had very few number of stations. Years of accumulated coda envelopes from data from different networks allowed to expand the envelope data base. It should be noted here that the definition of coda calibrations can be done using various advanced techniques, however we are using the power of simple description of the coda start and decay parameters to be able to various networks with few or higher number of stations. The following outlines the calibration method and more in-depth information can be found in Mayeda et al., [22].

The coda envelope Ac(f,t,r) is defined as:

$$A_c(f,t,r) = W_0(f).S(f).T(f).P(r,f).H\left(t-\frac{r}{v(f,r)}\right).\left(t-\frac{r}{v(f,r)}\right)^{-\gamma(f,r)} \exp\left[-b(f,r).\left(t-\frac{r}{v(f,r)}\right)\right] \quad (1)$$

where f is the center frequency, r is the epicentral distance in kilometers, t is the time in seconds from the origin time, v is the peak velocity, W_O represents the S-wave source, T represents the S-to-coda transfer function, S is the site effect, P includes the effects of geometrical spreading and attenuation, H is the Heaviside step function, γ(r) and b(r) are the distance-dependent coda shape factors that control the coda envelope shape. By ignoring the source, path, site and transfer function effects, the equation becomes

$$log_{10}\left[A_c(f,t,r).\left(t-\frac{r}{v(f,r)}\right)^{\gamma(f,r)}\right] = log_{10}\left[H\left(t-\frac{r}{v(f,r)}\right)\right] + b(f,r).\left(t-\frac{r}{v(f,r)}\right).log_{10}(e) \quad (2)$$

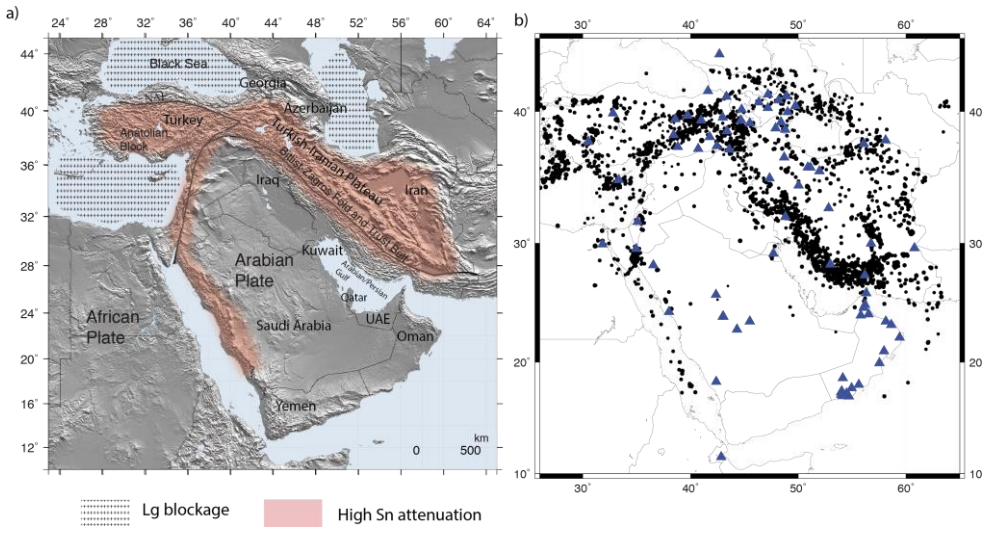

Figure 1. a) Tectonic setting and Lg, Sn propagation in the region (NAF: North Anatolian Fault Zone). Thick gray line is the plate boundary. b) Events (solid circles) and stations (blue triangles) that were used in this study. Magnitudes will be available as supplementary material.

We start with forming 13 narrowband envelopes of instrument corrected horizontal components (N-S and E-W) at epicentral distances ranging between 1° to 14°. The frequency bands we used in this study 0.03-0.05, 0.05-0.1, 0.1-0.2, 0.2-0.3, 0.3-0.5, 0.5-0.7, 0.7-1.0, 1.0-1.5, 1.5-2.0, 2.0-3.0, 3.0-4.0, 4.0-6.0 and 6.0-8.0Hz. The Hilbert transforms of envelopes were smoothed at varying number of samples (higher smoothness factor, h=10 at low frequencies gradually decreasing down to, h=2 for the highest frequency band). We then measure the maximum peak velocity within the group velocity window of 4.7-2.3 km/s for $\Delta > 300$km and 3.9-1.9km/s for $\Delta <= 300$km epicentral distance. The selection of the peak time of the direct phase is measured automatically by selecting the largest amplitude at Signal-to-Noise ratio 1.2 of the peak (Fig. 2). There are many false detections seen in unrealistic group velocity windows, however this low S/N is allowed to include many data points. Some of the peak velocity values are also the result of Sn to Lg conversions (4.0-4.3 km/s) at boundaries between oceanic and continental crust in the Mediterranean Sea, Black Sea and Caspian Sea. After measuring all the peak amplitude arrivals, we obtained the envelope peak velocity function that is represented with a simple hyperbola. This function will be part of coda calibration and will be used in future measurements in the region as well (red hyperbola in Fig. 2). The function is represented with,

$$v(f,r) = v_0(f) - \frac{v_1(f)}{v_{2(f)}+r} \quad (3)$$

where r is the epicentral distance and v_0,v_1 and v_2 are constants. In Fig. 2, four different frequency band peak velocities are shown. As the frequency gets higher the scattering of the shape parameter gets higher. At 0.3-0.5 Hz, it is dominated by surface waves (Rayleigh or Love) with an average velocity of around 3.0 km/s. At 0.7-1.0 Hz and 1.5-2.0 Hz, the predominant phase can be either Sn and Lg as clearly indicated with larger number of points accumulated around 4.5 km/s and 3.7km/s. At 3.0-4.0 Hz, the peak value is mostly dominated by Sn (4.5 km/s). Sn is observed with larger amplitude at high frequencies and the Lg amplitude is eliminated at higher frequencies. Coda envelope window lengths were determined by manual inspection of the time window of the envelope. All envelopes were carefully inspected in order to avoid the effects of the aftershocks. The expectation of minimum and maximum window length were adopted from previous studies [21; 39] and slightly modified for the region. The window lengths change as a function of frequency and depend on the attenuation

structure in the region. If the selected coda window length is too short then there is a bias of estimating the coda amplitude in the very early part of coda due to low S/N. Coda window tends to last very long for very large events (Mw > 7.0). We eliminate those cases by limiting the maximum window length criteria.

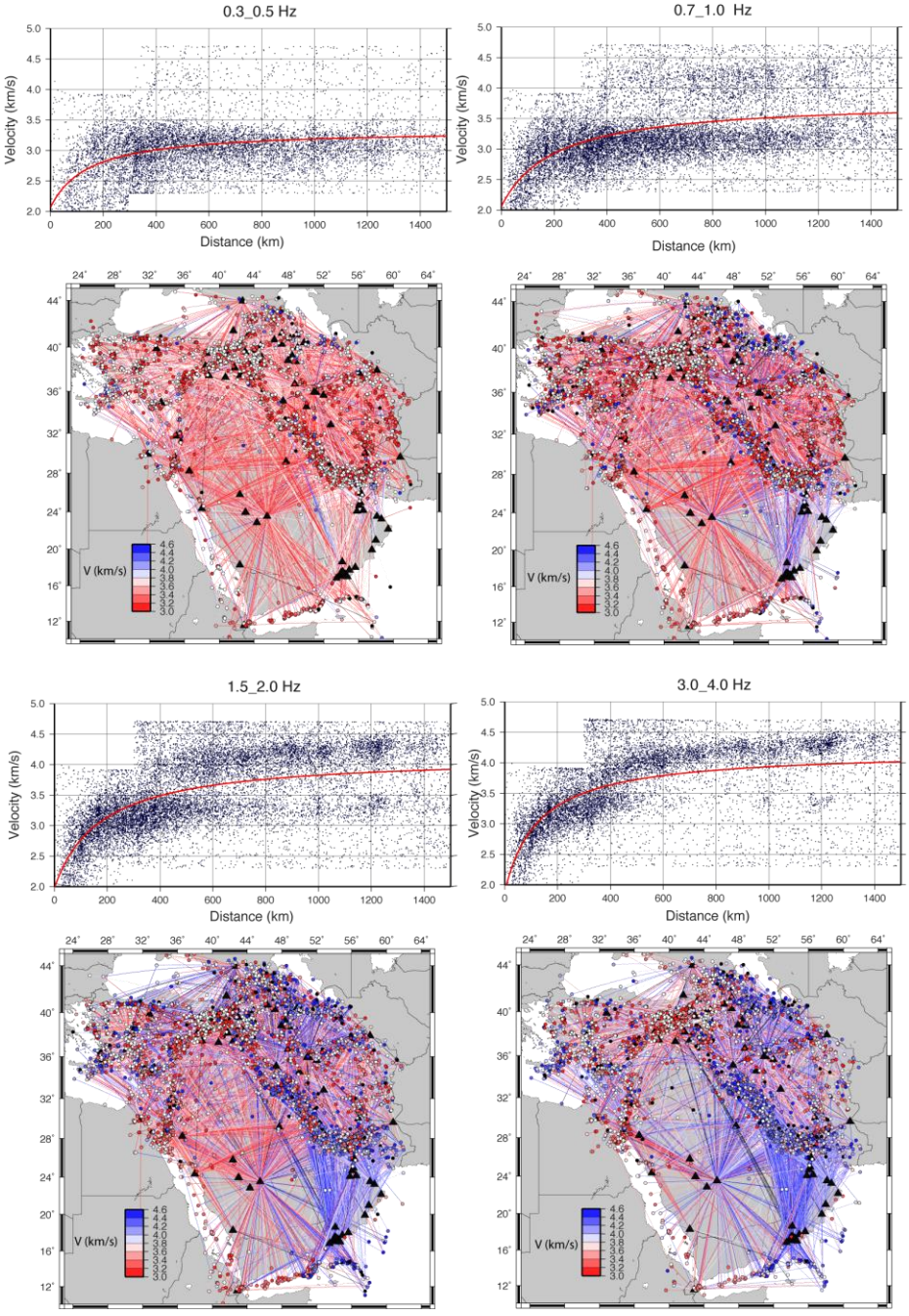

Figure 2. Automatically picked coda envelope peak velocity at selected frequency bands. Earthquakes are plotted as circles and color-coded for their velocities.

The shape of the coda envelopes are represented by a functional form

$$b(f,r) = b_0(f) - \frac{b1(f)}{b2(f)+r} \quad (4)$$

and

$$\gamma(f,r) = \gamma_0(f) - \frac{\gamma1(f)}{\gamma2(f)+r} \quad (5)$$

which have empirically proven to provide a reasonable fit of the envelopes as a function of increasing distance. Fig. 3 shows the b value and the estimated hyperbola (eq. 4) at four different frequencies. The coda shape parameter does not seem to scatter much at local to near-regional distances (<200 km) below 0.5-0.7 Hz. However, as frequencies increase the shape parameter seems to show increasing scatter at local distances. The 3.0-4.0 Hz band seems to exhibit very large variation and scatter at larger epicentral distances. We have fewer shape parameters than the peak values due to rejection for window lengths. Fig. 4 and 8 show these variations when compared to the synthetic envelopes.

Fig. 4 shows the observed coda envelopes along with empirical synthetic envelopes. Coda amplitudes are measured by DC shifting the synthetic envelopes that were created for a unit source. The envelope start and the shape functions were obtained from the hyperbolic functions (Eqs. 4 and 5). In Fig. 4, thick gray and black synthetic envelopes were shifted to fit the amplitude level and the coda measurements are made at 200 sec for all frequencies (Scott Phillips, personal communication). The rationale for choosing this particular lapse time is to sample the same scattered ellipsoid at particular time in the coda.

In Fig. 4a we show an event recorded at stations RAYN (Saudi Arabia) and Iran (ASAO) at 1.0-1.5 Hz frequency band. In Fig.4.b the synthetic envelopes at 825 km are shown for all frequencies. The shape functions and the start times are obtained from Table 1. Notice in particular that station ASAO has a peak velocity associated with Sn, while station RAYN has an Lg associated velocity. Given this, it is all the more remarkable that the shapes are otherwise similar except for an offset of 0.3 log units. Site term for RAYN at 1.0_1.5 Hz is 19.388 while it is 20.029 for ASAO (Table 1-Site). The difference of 0.641 in site terms accounts for much of this difference, with Q path variations accounting for the rest.

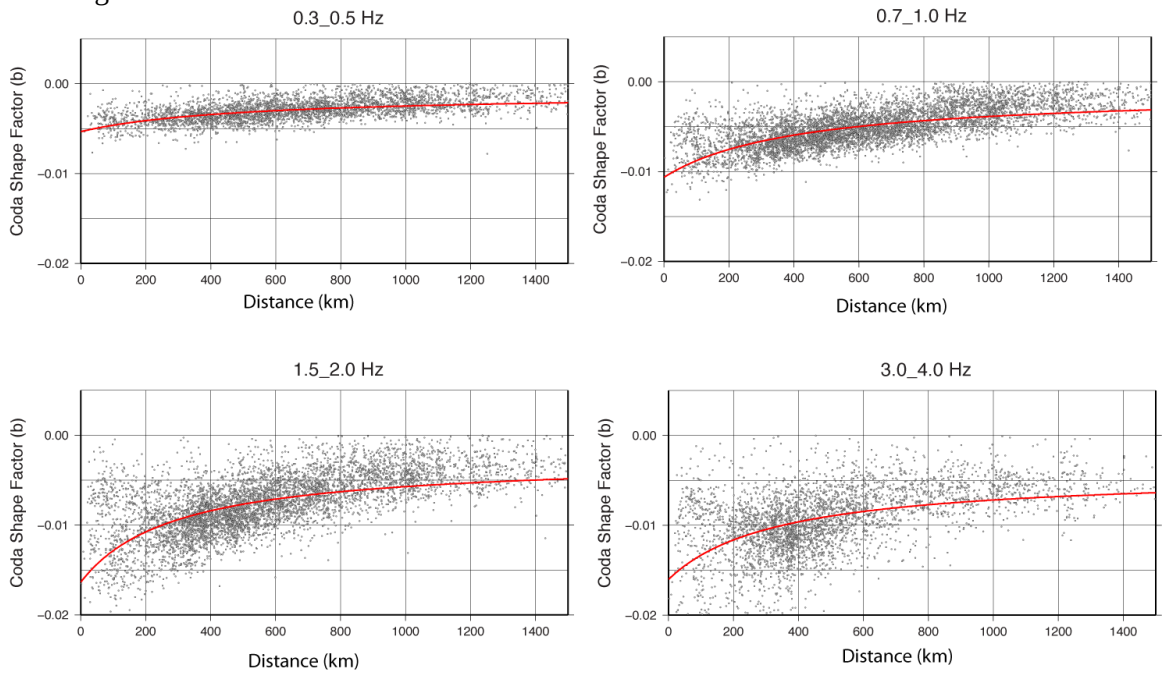

Figure 3. Coda shape function (parameter b, equation 4) at selected frequencies.
Note the higher scatter at higher frequencies and higher frequency local distances scatters.

Frequency band(Hz)	v0	v1	v2	b0	b1	b2	Y0	Y1	Y2	p1	p2	xc	xt	Q	site
0.03_0.05	3.10	12	201	-0	0.18	500	0.10	0	1	0.0000	1	1000	1.58	998710.8	21.98
0.05_0.1	2.95	14	201	-0	0.00	0	0.10	0	1	0.1320	1	829	1.33	996396.4	21.02
0.1_0.2	2.85	64	200	-0	0.52	500	0.10	-1	1	0.0639	1	496	2.88	263.153	20.42
0.2_0.3	3.25	250	201	-0	1.56	499	0.10	0	1	0.2554	1	414	3.61	203.628	19.76
0.3_0.4	3.35	186	145	-0	2.14	500	0.10	0	1	0.6921	1	536	1.00	306.921	18.65
0.5_0.7	3.55	284	199	-0	3.94	500	0.10	0	1	0.6162	1	704	1.00	323.646	19.00
0.7_1.0	3.80	350	201	-0	4.00	417	0.10	0	1	0.1932	1	190	4.06	470.448	19.85
1.0_1.5	4.05	400	199	-0	4.00	291	0.10	0	1	0.0522	1	265	3.25	704.315	20.29
1.5_2.0	4.15	380	175	-0	4.00	291	0.10	0	1	0.0092	1	144	2.83	1293.358	20.50
2.0_3.0	4.20	342	151	-0	4.00	276	0.10	-19	10	0.0088	1	417	17.34	1392.955	20.60
3.0_4.0	4.20	298	129	-0	4.00	338	0.10	-41	22	0.1238	1	1000	1.23	1247.04	20.60
4.0_6.0	4.15	246	107	-0	4.00	342	0.10	-51	30	0.3361	1	1000	1.69	2395.534	20.24
6.0_8.0	4.00	174	79	-0	4.00	337	0.10	-50	41	0.0000	1	466	2.46	3220.568	21.45

Table 1. Coda calibration (1-D) parameters for UOSS station.
Note that only last column (the site term) varies by station (Supplementary material).

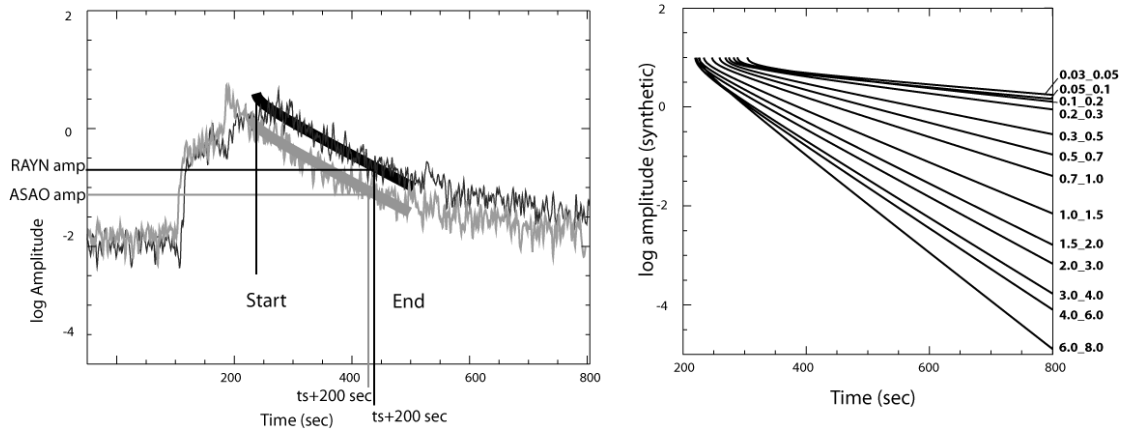

Figure 4. An example of synthetic envelopes at 825 km distance is shown at the right panel. The start time and the shape functions were obtained from Table 1. An example March 22.2005 event (Mw=4.21) envelopes for 1.0_1.5 Hz frequency band is shown for ASAO (gray) and RAYN (black) and the synthetic (thick black and gray lines) (event from Figure 11a SZ).

After all the amplitudes are collected from 74 stations at 13 frequency bands we corrected for path effect. It has generally been observed that attenuation of coda varies with frequency, tectonic region, and the lapse time interval used in the observations to be lower in tectonically seismic active regions and higher in seismic inactive stable regions [36, 14, 15]. We used the extended Street and Herrmann (ESH) a modified Street et al. (1975) formulation where both the geometrical spreading and the Q effect are corrected. The formulation, approach, corrects for the geometrical spreading, and its results are more stable than those derived from using the Brune-like corrections at higher frequencies [28; 39]. Instead of one critical distance, they define a distance range where the transition changes smoothly (Fig. 5).

$$f(r) = r^{-p1} \qquad r < X_1$$
$$f(r) = (X_1{}^{-p1})(r/X_1)^{\,p1+\Delta p(r)/2} \quad X_1 < r < X_2$$

where (6)

$$\Delta p(r) = \log(r/X_1)(p2 - p1)/\log(X_2/X_1)$$
$$f(r) = (X_1{}^{-p1})(X_2/X_1)^{-(p1+\Delta p(r)/2)}\,(r/X_2)^{-p2} \qquad r > X_2$$

Where $\Delta p(r) = (p_2 - p_1)$

To minimize the inter-station scatter between the stations, the inversion algorithm is applied using the following relations,

$$X_1 = X_c/X_t X_2 = X_c \times X_t$$

X_c is the critical distance and X_t is the transition term. These terms and the *p1*,*p2* are provided at Table 1. As shown in coda shape parameter plots, scattering of the coda shape function is higher at local distances (x< 200km) specifically at higher frequencies which indicates a difference between local S wave coda and regional Lg coda. In order to account these variations the ESH technique has been proven to improve the inter-station amplitude variations [28; 39].

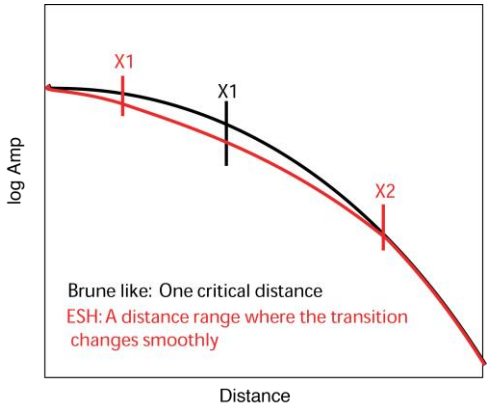

Figure 5. A comparison of to the Extended Street and Herrmann (ESH) formulation (red) with two critical distances to a single critical distance (black).

We have determined the path correction by inverting the measured coda amplitudes for three solved parameters (a1, a2 and X1), and where the second critical distance (X2) is fixed (Fig. 5). Fig. 6 shows one frequency band and the path distribution where we obtained those correction parameters. The number of paths are more limited than the number of paths shown in Fig. 2 due to earthquake distribution, rejected measurements or not having enough measurement for a common earthquake recorded by two or more stations. The majority of paths are within the 500-800km distance range.

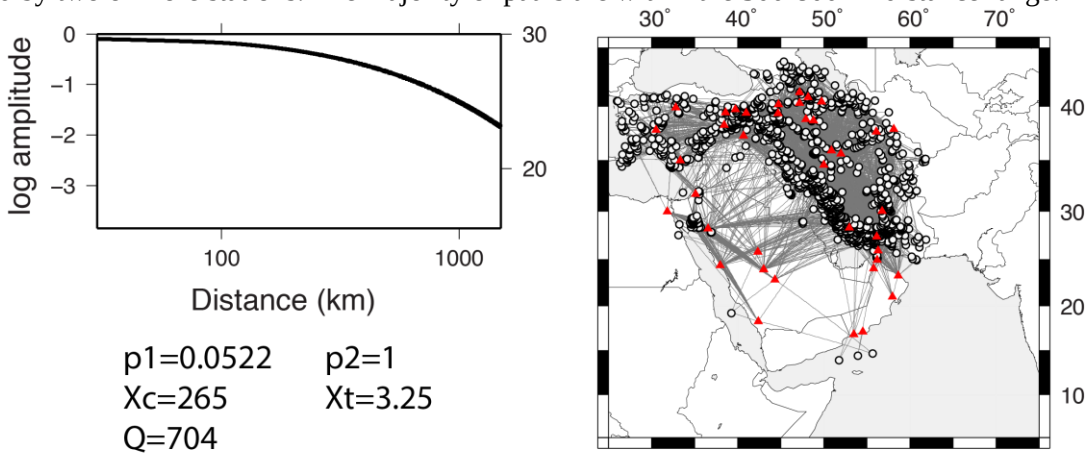

Figure 6. 1-D path (ESH) correction curve for frequencies 0.7-1.0 Hz with the path coverage on the right.

We apply these empirical corrections to the coda amplitudes in each frequency and obtain a "dimensionless" amplitudes. The next step is to tie this to a known Mw measurements calculated in the region through independent techniques such as 1-D long-period waveform modeling. Fig.7 illustrates how "S-to-coda transfer" is applied to obtain site-terms using station UOSS and 360 source spectra. We use moment estimates from Gene Ichinose (personal communication) and Covellone and Savage (2012).

Ichinose uses a specific velocity model to the region for waveform inversion, while Covellone and Savage (2012) use an adjoint tomography where they improved the model during moment tensor inversion. We compared common events obtained using both techniques to examine any bias. The Mw's were quite consistent without any bias and less scatter. It is known that if an unrepresentative the regional velocity model can cause under or overestimation of the moment value [32]. We believe that these 168 independently waveform-modeled events are reliable estimates of the moment magnitudes in the Middle East region (Fig. 9).

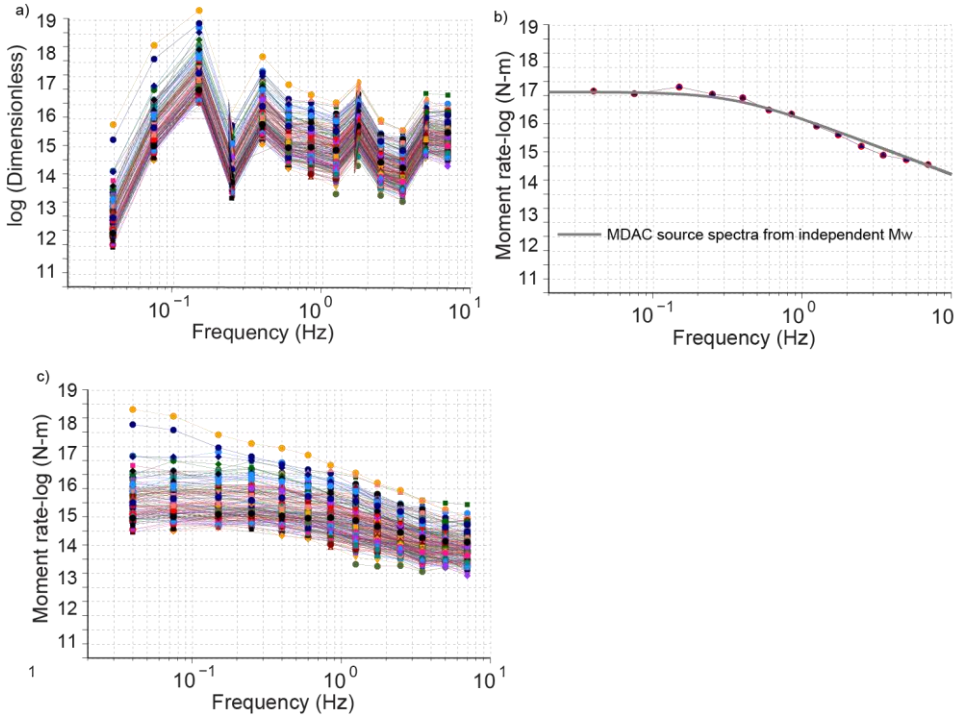

Figure 7. a)Source spectra site corrections are illustrated using 300 path-corrected amplitudes at station UOSS b) One independent waveform modeled event is shown as an example out of 168 calibration events that contributed to the site corrections (Table 1) c) moment rate spectra of the corrected amplitudes. Note the higher corner level of small events.

A theoretical source spectra created using MDAC (Magnitude, Distance, Amplitude Correction) [38] formulation and the site correction is applied at each frequency band using the waveform modeled events (Fig.7). The MDAC methodology creates a synthetic moment-rate spectra using simple one-dimensional propagation model and earthquake source model to observed regional seismic spectra. We used MDAC parameters where the apparent stress, and reference moment are 3 bars and 0.30×10^{16} N-m, respectively. Obviously a bias can be introduced during calibration. For now we ignore these effects since the effect will be observed in higher frequency portion of the source spectra.

Results

We obtained moment magnitude estimates of 2,900 crustal events in the Middle East region using the 1-D coda calibration, where the calibration parameters are listed in Table 1. Our range of magnitudes span small to larger size events (3.5<Mw<7.0). Coda Mw's are obtained by fitting the MDAC spectra. As shown in velocity peak values in Fig. 2, our fitted hyperbola (red line) is averaging the distributed Sn and Lg phase velocities specifically at frequencies between 0.7-1.5 Hz. This may clearly introduce an error in our measurements. To illustrate the possible effect of this issue we show the November 11, 2006 Mw=4.09 as an example of fit at various frequencies using coda calibration technique (Fig. 8, 10b). Stations KRBR and GRMI are at similar epicentral distances but GRMI path travels along the northern Zagros (where Sn is observed) whereas GRMI travel through the southern Iranian Plateau. Similar to Fig. 4 we see variations in the synthetic envelopes. This variation however does not show a very significant effect on the source spectra (Fig.10b) below 0.7 Hz. In some cases like Fig.10 a shows more variation at higher frequencies which might be due to 2-D attenuation effect. Instead of limiting our MDAC fit to the observed moment-rate-spectra below certain frequency we fit the full spectra and document the frequency range that the spectra (thus Mw) is calculated from.

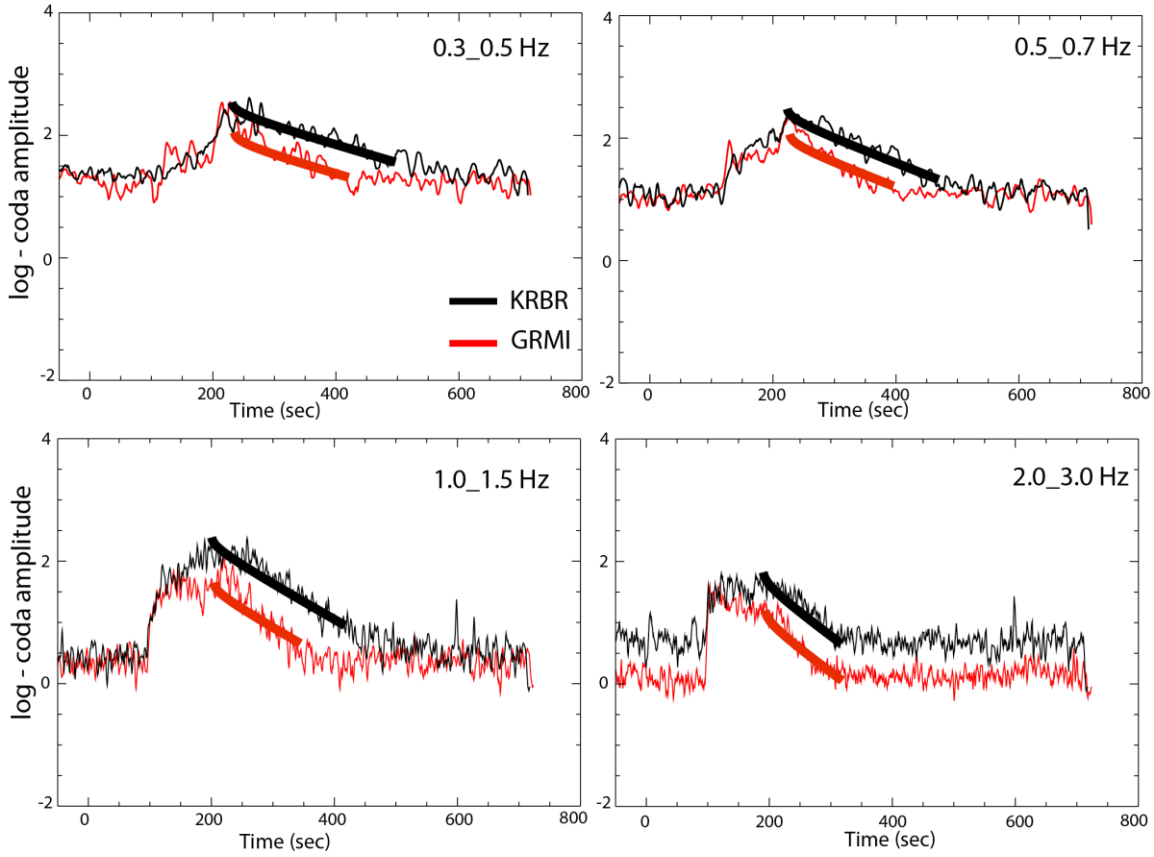

Figure 8. Synthetic and raw coda envelopes are displayed for four frequency bands. In order to illustrate the coda shape effect we picked two stations that are fairly close in their epicentral distances, KRBR is 721 km and GRMI- 732 km. Here we see that for the higher frequencies the fitting of the envelopes is degraded, as is the timing because the peak velocity is somewhat of an average between Sn and Lg peak velocities. (Figure 10b Central Zagros(CZ)).

Nonetheless, the flat part of the moment-rate spectra where the Mw is measured at the long-period level of the spectra is around 1 Hz for Mw ≥~3.5. The comparison of 168 calibration events with coda-derived Mw's is shown in Fig. 9. Higher scattering is observed at 4.0<Mw <5.0 and this is expected due to variations of regional coda shapes and amplitudes having a strong 2-D effect on coda. Nonetheless, the correlation is high, does not show much scatter, and no bias is observed. Standard deviation of single station spectra is calculated for these calibrations events and the results are shown in Fig.9b. The average standard deviation is 0.25 for frequencies between 0.03 to 0.5 while it increases as high as 0.4 at frequencies greater than 0.7 Hz.

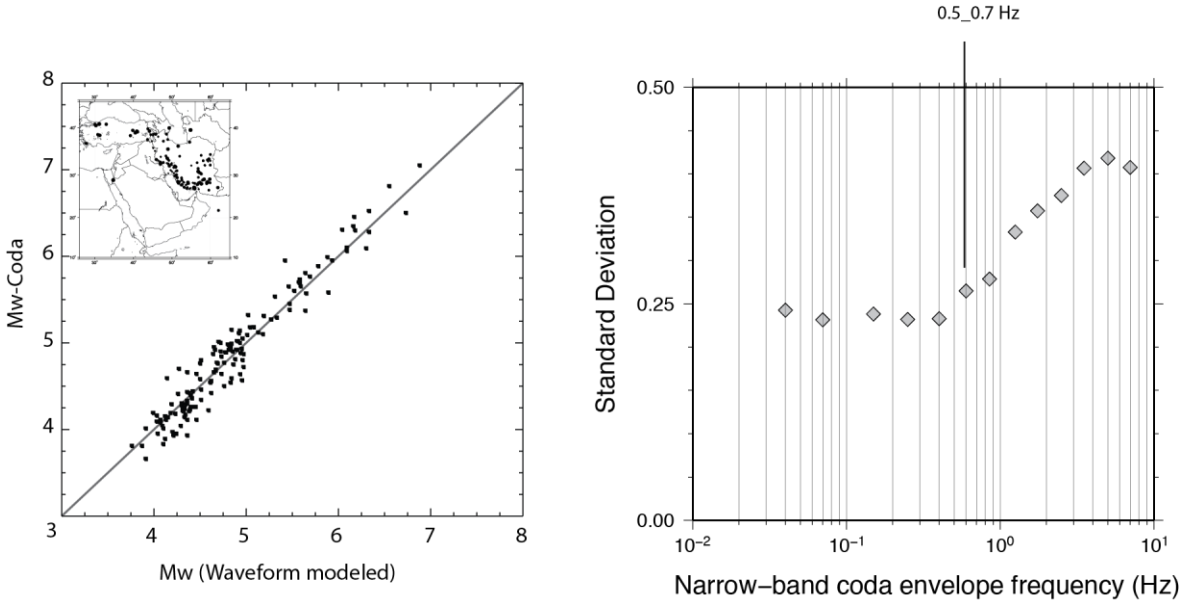

Figure 9. a) Coda Mw comparison with waveform modeled Mw b) Standard deviations grouped indifferent frequency bands. At frequencies higher than 0.7 Hz it is more likely to get higher scatter due to 2-D effects on coda envelopes and mixing of Sn-coda and Lg-coda.

Results of four selected events representing selected regions are shown in Fig.10. Fig.10a source spectra is selected from the Southern Zagros (SZ). Dotted gray line is the MDAC spectra for an Mw=4.21 event. Four different stations are located in the Zagros, Makran and the Arabian/Persian Gulf at few hundred kilometers to larger epicentral distances. Source spectra from individual stations show scatter above 1.0 Hz. Fig.10b is from an event in Central Zagros (CZ) where the recording stations span most of the Iranian Plateau. This event Mw=4.09 event that does not have many high frequency measurements due to strong attenuation. The source spectra shown in Fig.10c are from an event in the Caucasus. It is recorded by the Iranian, Turkish and GSN(IRIS) stations. High-frequency scatter of source spectra is now larger for this event above 0.5_0.7 Hz. The paths to this event span through the Greater Caucasus (KIV), Lesser Caucasus (AGRB), Anatolian Plateau (VANB, URFA) and the Iranian Plateau (NASN, SHGIR, GHIR). The independent waveform modeling Mw solution of this event is overestimated at 5.01. Our coda calibration results very consistently estimates Mw=4.70. If the regional models are inappropriate or 3-D variations are strong, the regional moment-tensor solutions can be significantly affected. The last example shows an event from Eastern Turkey. The IRIS-PASSCAL deployment in eastern Turkey recorded this event as well as the GSN-IRIS stations (KIV, ISP, CSS). For this event, the source spectra show larger variation above 0.5 Hz. The path to CSS travels partially through the Mediterranean. This may cause a conversion at the continental/oceanic crust boundary [12].

a)

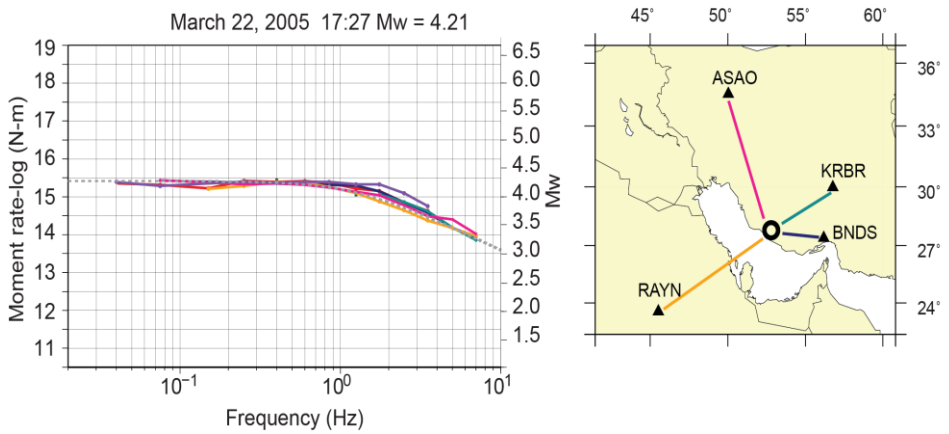
March 22, 2005 17:27 Mw = 4.21
Moment rate-log (N-m)
Frequency (Hz)
Mw
ASAO
KRBR
BNDS
RAYN

b)

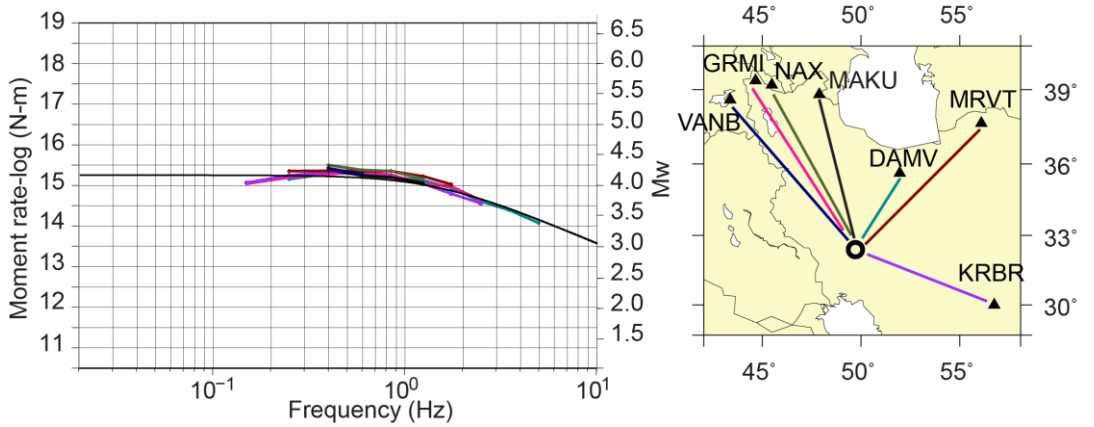
Nov 11, 2006 02:19 M= 4.09
Moment rate-log (N-m)
Frequency (Hz)
Mw
GRMI
NAX
MAKU
MRVT
VANB
DAMV
KRBR

c)

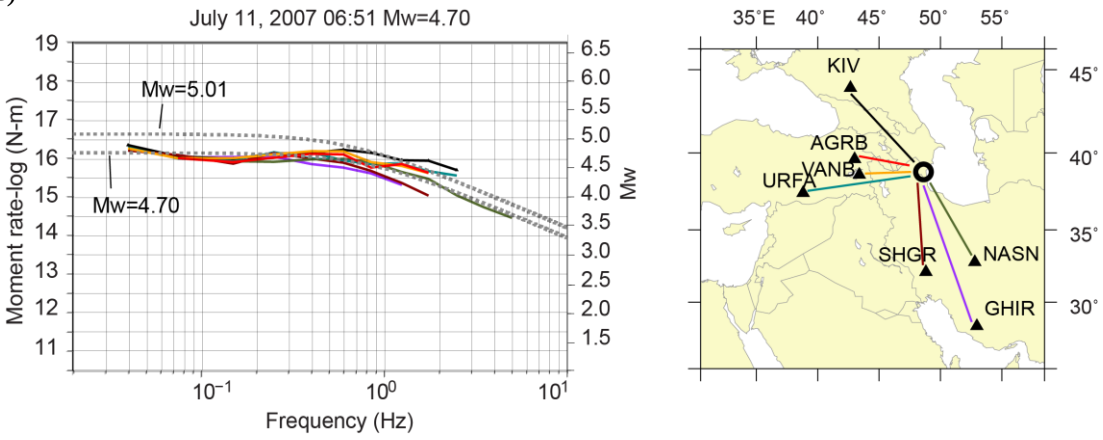
July 11, 2007 06:51 Mw=4.70
Moment rate-log (N-m)
Frequency (Hz)
Mw
Mw=5.01
Mw=4.70
KIV
AGRB
VANB
URFA
SHGR
NASN
GHIR

d)

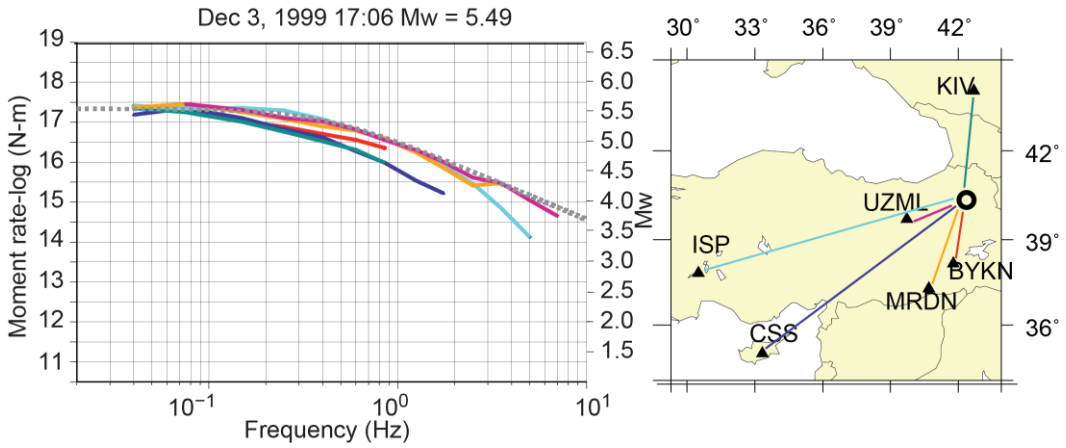

Figure 10. Selected 4 events with source spectra at individual stations shown with source spectra from calibrated events at a) Southern Zagros (SZ) , b) Central Zagros (CZ), c) Caucasus- Caspian (CC) and d) Eastern Turkey (ET). Magnitudes shown at panels are derived from coda envelopes. The gray dotted line is MDAC theoretical source spectra.

Standard deviations that are shown in Fig.9b will be the basis for error bounds for the magnitudes that we will be providing as a supplementary material. At the table of magnitudes we provide the frequency range for the source spectra where Mw is measured, number of frequency bands, number of stations for each event so that the magnitude of interest will be carefully evaluated. Due to limited number of stations in the early years, we kept the minimum number of station criteria at least one and minimum number of frequency at each spectra to be four. The magnitude for each event is obtained by averaging the source spectra at each individual frequency (Appendix 1).

Conclusion

Although we observe significant variations in the seismograms throughout the region, the 1-D coda method has shown the ability to provide stable moment estimates for frequencies below ~0.7Hz and subsequently is ideal for the moderate to large magnitude events (~3.5<Mw<7.0). Even so, the robustness of the technique allowed us to measure Mw's down to 2.0, but with increasing variations at higher frequencies (Fig.9b) we prefer not to provide any magnitude below 3.5 in this study. In addition, shorter coda length for smaller events may no longer be back scattered but is dominated by more forward multiple scattering. We are aware of the limitations for smaller events, short window length at high frequencies and we provide the range of frequencies for cautious use of specifically smaller events. With the limited amount of moment magnitudes available, this study will provide first time moment magnitudes of smaller events in the region.

In an accompanying paper (Pasyanos et al., 2015) we will be using the 1-D coda calibrations to provide coda amplitudes that can be inverted for 2-D attenuation structure. The variable attenuation structure can be used to robustly estimate the magnitudes of small events using only high frequencies and at only a few or single path.

Local magnitudes of national networks and Probabilistic Seismic Hazard Assessment (PSHA) studies often require stable Mw measurements in order to obtain the completeness and harmonization of the catalogs [30]. We derived the connection between M_L, M_b and M_s magnitudes. Since each magnitude reported on a catalog had often several organizations on it we use the median value from the available catalogs. Instead of a least squares fit to the data, which requires that the uncertainty on the independent variable (i.e. M_L, M_b and M_s) is at least one order of magnitude smaller than the one on the dependent variable (i.e. Mw), we utilize orthogonal regression, which allows both the

dependent and independent variables to be affected by uncertainty [7, 18]. Fig. 11 shows the connection between these magnitudes. The red line is the orthogonal fit and is shown along with the dashed line which is a linear fit.

One of our goals in this paper is to help in operational needs of national networks in the Middle East region. With developing networks and seismic data availability, regional models are improving but still not quite adequate to predict Green's functions to be used for regional moment tensor inversion and moment magnitude studies. At LLNL, we have developed java based The Seismic WaveForm Tool (SWFT) computer code to speed the measurement of Mw's through existing coda calibration technique. The code is available upon request and uses Seismic Analysis Code (SAC) format data. The calibration presented here will help local monitoring organization for rapid moment magnitude solution.

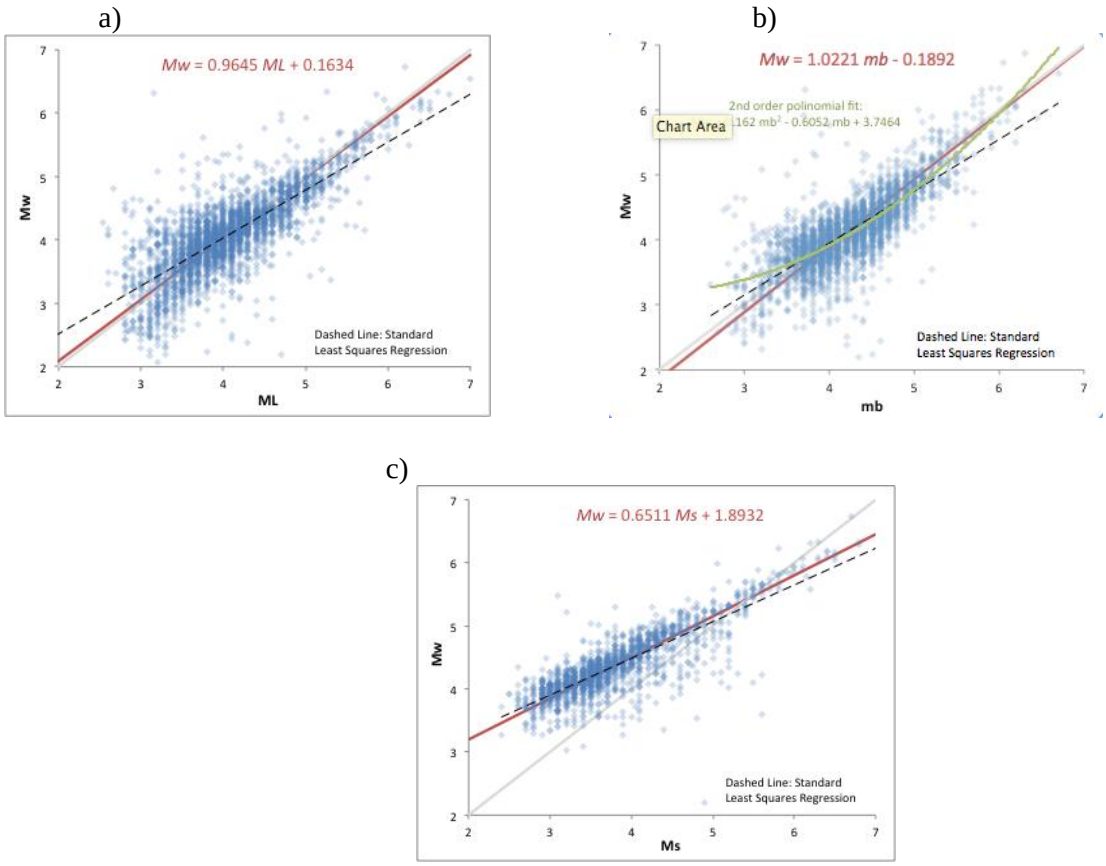

Figure 11. Connection between codaM_L, $M_b$and M_s. The red line and the equation in red is the orthogonal fit, the black dashed-line is a linear fit. The green line shows the second order polynomial fit only for M_b- M_w.

Data and Resources

Data is obtained from IRIS-PASSCAL deployments, IIEES (Iranian Institute of Earthquake Engineering), Republican Seismic Survey Center of Azerbaijan (RSSC), Earthquake Monitoring Center (EMC) of Sultan Qaboos University, KACST (King Abdullah City of Science and Technology), Kandilli Observatory and Earthquake Research Institute (KOERI), Kuwait Institute for Scientific Research (KISR) and Saudi Geological Survey (SGS)

Acknowledgements.

Majority of the openly available data is obtained from Incorporated Research Institutions in Seismology (IRIS). Plotting is done using Generic Mapping Tool (GMT) macros. This work was performed under the auspices of the U.S. Department of Energy by Lawrence Livermore National Laboratory under Contract DE-AC52-07NA27344. This study is partially supported by AFRL FA9453-11-C-0235 and DE-AC52-07NA27344/LL11-BAA11-13-NDD03. This is LLNL contribution LLNL-JRNL-679299.

REFERENCES

[1] Abercrombie R.E. Earthquake source scaling relationship from 1 to 5 ML using seismograms recorded at 2.5 km depth, *J. geophys. Res.*, 100, 1995, pp.24 015–24 036.

[2] Aki K., (1966). Generation and propagation of G waves from the Niigata earthquake of June 16, 1964. Part 2. Estimation of earthquake moment from the G wave spectrum, *Bull. Earthquake Res. Inst.* Tokyo Univ., 44, pp.73–88.

[3] Aki, K. and B. Chouet. Origin of coda waves: Source, attenuation, and scattering effects, *J. Geophys. Res.*, **80,** 1975, pp.3322–3342.

[4] Al-Damegh K., Sandvol E., Al-Lazki A.I., and Barazangi M. Regional seismic wave propagation (Lg and Sn) and Pn attenuation in the Arabian plate and surrounding regions. *Geophys. J. 2004, Int*.; pp.157:775-795.

[5] Al-Damegh K., Sandvol E., Al-Lazki A., Barazangi M., Regional seismic wave propagation (Lg and Sn) and Pn attenuation in the Arabian plate and surrounding regions, *2004. Geophys. J. Int., pp.157, 775–795.*

[6] Baumgardt, D. R. Sedimentary basins and the blockage of Lg wave propagation in the continents, *Pure Appl. 2001*, *Geophys*., pp.158, 1207-1250.

[7] Castellaro, S., F. Mulargia and Y.Y.Kagan. Regression problems for magnitudes. 2006, Geophys. J. Int. pp.165: 913–930.

[8] Cong, L. and B. Mitchell. Lg coda Q and its relation to the geology and tectonics of the Middle East. *Pure Appl.1998, Geophys*. pp.153: 2–4, 563–585.

[9] Covellone B., and Savage B. A quantitative comparison between 1D and 3D source inversion methodologies: application to the Middle East. 2012, *Bull. seism. Soc. Am*. pp.102(5):2189 2199.[10] Eken, T., K. Mayeda, A. Hofstetter, R. Gok, G. Orgulu, and N. Turkelli, An application of the coda methodology for moment-rate spectra using broadband stations in Turkey, 2004, *Geophys. Res. Lett.*, 31, L11609, doi:10.1029/2004GL019627.

[11] Favreau P., and Archuleta R.J. Direct seismic energy modelling and application to the 1979 Imperial Valley earthquake, 2003, *Geophys. Res. Lett*., pp. 30, 1198.

[12] Gok, R., N. Turkelli, E. Sandvol, D. Seber, and M. Barazangi, Regional Wave propagation in Turkey and surrounding regions, *Geophys. Res. Lett*., 27(3), pp. 429–432, 2000.

[13] Gok, R., E. Sandvol, N. Turkelli, D. Seber, and M. Barazangi, Sn attenuation in the Anatolian and Iranian plateau and surrounding regions, *Geophys. Res. Lett*., 30(24), 2003, 8042, doi:10.1029/2003GL018020.

[14] Jin, A. and K. Aki. Spatial and temporal correction between coda Q and seismicity in China, *Bull. Seismol. Soc. Am.*, 78, 1988, pp.741–769.

[15] Jin, A. and K. Aki, High-resolution maps of coda Q in Japan and their interpretation by the brittle-ductile interaction hypothesis, *Earth Planets Space*, 57, 2005, pp.403–409.

[16] Kadinsky-Cade, K., Barazangi, M., Oliver, J. and Isacks, B., Lateral variations of high-frequency seismic wave propagation at regional distances across the Turkish and Iranian Plateaus. *J. Geophys. Res*. 86: doi: 10.1029/JB080i010p09377. issn: 0148-0227, 1981.

[17] Kaviani, A., E. Sandvol, X. Bao, G. Rumpker, and R. Gok. The Structure of the Crust in the Turkish-Iranian Plateau and Zagros using Lg Q and Velocity, Geophys. J. Int., 200 (2): 1254-1268doi: 10.1093/gji/ggu468, 2015.

[18] Kendall, M.G. & Stuart, A. The Advanced Theory of Statistics, Vol. 2, 4th Ed., Griffin, London. 1979.

[19] Malagnini, L., Mayeda, K., Akinci, A. & Bragato, P.L. Estimating absolute site effects, *Bull. seism. Soc*. Am., 94, 4, pp.1343–1352, 2004.

[20] Mayeda K. m_b (L_g coda): A stable single station estimator of magnitude, *Bull. seism. Soc. Am.*, pp.83, 851–861, 1993.

[21] Mayeda K., and Walter W.R.. Moment, energy, stress drop, and source spectra of western United States earthquakes from regional coda envelopes, *J. geophys. Res*., pp.101, 11 195–11 208, 1996.[22] Mayeda K., Hofstetter A., O'Boyle J.L., and Walter W.R. Stable and transportable regional magnitudes based on coda-derived moment-rate spectra. *Bull. seismol. Soc. Am*., pp.93, 224–239, 2003.

[23] Mayeda K., Dreger D., Walter W.R., Wurman G., and Tajima F. BDSN calibration for Northern California earthquakes from coda-derived source spectra: moment magnitude and radiated energy, *Seism. Res. Lett.*, pp.75, 278, 2004.

[24] Mayeda, K., and L. Malagnini. Source radiation invariant property of local and near-regional shear-wave coda: Application to source scaling for the Mw 5.9 Wells, Nevada sequence, *Geophys. Res. Lett*. 37, L07306, doi:10.1029/2009GL042148, 2010.

[25] Mitchell B.J., Pan Y., Xie J., Cong L. Lg coda Q variation across Eurasia and its relation to crustal evolution. 1997, *J. geophys. Res*. ;102(B10):22 pp.767-22 779.

[26] Mitchell, B. J. and L. Cong. Lg coda Q and its relation to the structure and evolution of continents: A global perspective, 1998, *Pure Appl. Geophys.*, pp.153, 655–663.

[27] Molnar, P., and J. Oliver, Lateral variations of attenuation in the upper mantle and discontinuities in the lithosphere, 1969, *J. Geophys. Res.*, 74, pp.2648-2682.

[28] Morasca P, Mayeda K, Malagnini L, Walter WR.Coda derived source spectra, moment magnitudes, and energy-moment scaling in the Western Alps. 2005, Geoph J Int 160(1): pp.263–275.

[29] Morasca, P., K. Mayeda, R. Gok, W. S. Phillips, and L. Malagnini. 2D Coda and Direct-Wave Attenuation Tomography in Northern Italy, 2008, *Bull. of the Seismol. Soc. of America*, 98.4: pp.1936-946.

[30] Onur T., Gok R., H. Mahdi, and H. Al-Shukri. Unified seismic catalog of Iraq, *submitted to Pure Appl. Geophys.2015*.

[31] Pasyanos, M.E., R. Gok, and W.R. Walter. 2-D variations in coda amplitudes in the Middle East, *submitted* to *Bull. Seism. Soc. Amer*. 2015.

[32] Patton, H.J. and G.E. Randall. On the causes of biased estimates of seismic moment for earthquakes in central Asia,2002, *J. Geophys. Res.*, 107, doi:10.1029/2001JB000351.

[33] Phillips, W. S. and K. Aki. Site amplification of coda waves from local earthquakes in Central California, 1986, *Bull. of the Seismol. Soc. of America*, 76, pp.627–648.

[34] Rodgers, A. J., J. F. Ni, and T. M. Hearn. Propagation characteristics of short-period Sn and Lg in the Middle East, 1997, *Bull. Seismol. Soc. Am.* 87: pp.396–413.

[35] Sandvol, E., K. Al-Damegh, A. Calvert, D. Seber, M. Barazangi, R. Mohamad, R. Gok, N. Turkelli, and C. Gurbuz. Tomographic imaging of Lg and Sn propagation in the Middle East, 2001, *Pure Appl. Geophys*., 158, 1121–1163, doi:10.1007/PL00001218.

[36] Singh, S. and R. B. Herrmann. Regionalization of crustal coda Q in the continental United States, 1983, *J. Geophys. Res.*, 88, pp.527–538.

[37] Street, R. L., Herrmann, R. B., and Nuttli, O. W. Spectral characteristics of the Lg wave generated by central United States earthquakes, 1975, *Geophys. J. Roy. Astron. Soc. 41, pp.51-63.*

[38] Walter, W.R. and S.R. Taylor. A revised Magnitude and Distance Amplitude Correction (MDAC2) procedure for regional seismic discriminants: theory and testing at NTS, Lawrence Livermore National Laboratory, 2001, UCRL-ID-146882, 13 pp.

[39] Yoo, S.-H., J. Rhie, H.-S. Choi, and K. Mayeda. Coda-derived source parameters of earthquakes and their scaling relationships in the Korean Peninsula, 20011, *Bull. Seismol. Soc. Am.* 101, pp.2388–2398, doi: 10.1785/0120100318.